Geomorphology 491 (2025) 110031

Contents lists available at ScienceDirect

Geomorphology

journal homepage: www.elsevier.com/locate/geomorph

Field assessment of the wind speed-up from the two modes of dune orientation

Ping Lü [a], Clément Narteau [b,*], Fang Ma [c], Jeanne Alkalla [b], Zhibao Dong [a]

[a] School of Geography and Tourism, Shaanxi Normal University, Xi'an, 710119, Shaanxi, China
[b] Université Paris Cité, Institut de physique du globe de Paris, CNRS, 1 rue Jussieu, 75238, Paris cedex 05, France
[c] School of History, Culture and Tourism School, Fuyang Normal University, Fuyang, 236037, Anhui, China

ARTICLE INFO

Keywords:
Wind speed-up
Dunes
Migration
Elongation

ABSTRACT

Since a multidirectional wind regime can lead to the development of two types of dune with different orientations, they can be used together to examine the permanent impact of dune topography on the increase in near-surface wind speed. Here we examine 30 months of wind data recorded in the Qaidam basin at the crest of a linear elongating dune with a longitudinal alignment, and a migrating barchanoid ridge with a transverse alignment. After synchronization, we compute the ratio between these wind speeds over the entire range of wind direction. The oscillating signal reflects the linear dependence of the wind speed-up on dune aspect-ratio, with a fractional speed-up ratio $\delta \approx 0.5$. Based on this value and climate reanalysis wind data, a theoretical model of dune dynamics accurately predicts the shape and orientation of local dunes, as well as the observed migration and elongation rates along with their respective directions. Such a quantification of active dune dynamics provides a common understanding of complex dune fields, facilitating both forward and inverse modeling in diverse environmental contexts.

1. Introduction

In order to study dune morphodynamics, it is essential to characterize the variation in sand flux along dune slopes, with a particular focus near the crest where the transport rate is the highest (Bagnold, 1941; Rubin and Hunter, 1987). Whatever the transport law under consideration, it depends mainly on near-surface wind speed, and therefore on the perturbations induced by dune topography on the flow. This feedback of dune shape on the flow is an issue shared by many disciplines, and, from mid-70s, there has been a theoretical formalism for predicting boundary layer flow over complex topography (see Finnigan et al. (2020) and references within).

The compression of streamlines causes the wind speed measured at a given height to be higher on the windward slope of an obstacle than on a flat bed away from any topography. This perturbation reaches a maximum close to the crest and is usually quantified by estimating the fractional speed-up ratio,

$$\delta = \frac{u_{\mathrm{crest}} - u_{\mathrm{flat}}}{u_{\mathrm{flat}}}. \tag{1}$$

Based on the analytic model of Jackson and Hunt (1975), which decomposes the near-surface flow vertically into an inner and an outer layer, it is generally accepted that this fractional speed-up ratio is directly proportional to the obstacle aspect-ratio,

$$\delta = \beta \frac{H}{\mathcal{L}}, \tag{2}$$

where H is the height of the obstacle, and β a dimensionless coefficient that takes into account different physical ingredients (e.g., precise shape of the obstacle, roughness, thickness of the inner layer) affecting the vertical wind profile (Britter et al., 1981). Because it is often difficult to define the position of the upstream foot of the dune precisely in the field or from topographical surveys, the dune length $\mathcal{L}$ is here defined as the horizontal distance from the crest to the half-height point, as is commonly done in the study of atmospheric flow. According to this convention, the β-value ranges from 0.8 to 3.2 in field measurements, wind tunnel experiments, and numerical simulations (Bradley, 1983; Taylor et al., 1987). The specific challenge when sediment transport occurs on bedforms remains to adapt this theoretical formalism to an evolving topography. This is particularly true for aeolian dunes under multidirectional wind regimes, for which the apparent dune slopes vary with wind direction and during crest reversals (Gao et al., 2021; Chen et al., 2022).

In active dune fields, the fractional speed-up ratio has been measured on various dune types, including transverse and reversing dunes,

* Corresponding author.
E-mail address: narteau@ipgp.fr (C. Narteau).

https://doi.org/10.1016/j.geomorph.2025.110031
Received 26 November 2024; Received in revised form 30 July 2025; Accepted 25 September 2025
Available online 30 September 2025

in different climatic contexts, in sand seas or along coastlines (Arens et al., 1995; Wiggs et al., 1996; Neuman et al., 1997; Walker and Nickling, 2003; Hesp et al., 2005; Baddock et al., 2007; Walker et al., 2009; Bauer et al., 2012; Claudin et al., 2013; Hesp et al., 2015; Walker et al., 2022; Daudon et al., 2024). The data confirms that the speed-up effect depends on the apparent dune aspect-ratio when the wind direction changes, with reported δ-values ranging from 0.5 to 2.5 (Parsons et al., 2004; Hesp et al., 2015; Schwarz et al., 2021). However, most field measurements are performed on a single dune and over a short time period, which limits the ranges of wind direction and dune morphology from which the fractional speed-up ratio can be determined. Furthermore, there is still a lack of data allowing the simultaneous comparison of wind disturbances on dunes of various shapes and orientations. This is essential in complex dune fields because these perturbations modulate the sand flux at the crest, and therefore the differences in growth rate and dynamics between the different dune types (Zhang et al., 2012; Courrech du Pont et al., 2014; Gunn, 2023; Vérité et al., 2025).

Based on field, laboratory, and numerical experiments, recent research has demonstrated that there are two mechanisms for dune growth (Courrech du Pont et al., 2014; Gao et al., 2015; Fernandez-Cascales et al., 2018; Lü et al., 2022), which are not only selecting the orientation of the dunes but also their shape and dynamics (Courrech du Pont et al., 2024). With no limit to sand availability, the bed instability prevails (Kennedy, 1963; Lü et al., 2021), and periodic dunes grow in height lining up in the direction for which normal-to-crest components of transport are maximum (Rubin and Hunter, 1987; Ping et al., 2014; Gadal et al., 2019). In areas of limited sand supply under multidirectional wind regimes, isolated dunes can also elongate in the direction for which these normal-to-crest components of transport cancel each other out (Lucas et al., 2014; Rozier et al., 2019). To estimate all these sand fluxes from wind data, and derive the associated dune shapes and dynamics (Courrech du Pont et al., 2024), the simplest solution is to consider an infinite linear dune with a triangular shape and symmetric slopes (Courrech du Pont et al., 2014). Then, Eqs. (1) and (2) give

$$u_{\mathrm{crest}} = u_{\mathrm{flat}}\left(1+\delta|\sin(\theta-\theta_D)|\right) = u_{\mathrm{flat}}\left(1+\beta\frac{H_{\mathrm{D}}}{\mathcal{L}_{\mathrm{D}}}|\sin(\theta-\theta_D)|\right), \qquad (3)$$

where θ is the wind direction, θ_D the observed dune orientation, H_{D} the dune height, and $\mathcal{L}_{\mathrm{D}}$ the dune length at half-height. This sinusoidal dependence has been observed in the field (Schwarz et al., 2021), but remains to be quantified according to the δ-value. To this end, we investigate here the simultaneous variation of wind speed at the crest of dunes with different orientations in a dune field where the two growth mechanisms coexist.

2. Study site and methods

Wind measurements were taken between 2017 and 2021 in a dune field located on the alluvial fan of the Nalinggele River, south of the Qaidam basin, on the foothills of the Eastern Kunlun range in the Tibetan Plateau, China (Fig. 1a). In this area, the primary wind blows mainly from spring to fall towards the southeast, along the Kunlun Range, which also steers the storm winds. The secondary wind is of katabatic origin. It blows northeastwards, from the surrounding mountains towards the Qaidam basin, throughout the year with the same intensity, mainly between sunrise and mid-morning. This results in a bimodal wind regime with a divergence angle greater than 90°, promoting the formation of periodic barchanoid ridges or isolated linear dunes, depending on sand availability. These two types of dunes exhibit two distinct orientations, respectively noted θ_{H} and θ_{E} (Fig. 1b), while migrating or elongating in the same general southeast direction (Supporting Information, Figure S1). They are all eventually leveled by the steep terraces and annual spring flooding of the Nalinggele River (Chang et al., 2017).

Two sonic anemometers were positioned at the same height of 2 m at the crest of two dunes separated by 4.4 km. The one to the northeast is a two-kilometer-long linear dune (WS_1, Fig. 1c, e). The other to the southwest is a 35 m long barchanoid ridge (WS_2, Fig. 1d, f). With a sampling frequency of 1 min, the synchronized wind speed and direction data are complete on both dunes from 6 June 2017 to 31 December 2019. To account for dune migration, the upper time limit was selected to ensure that the anemometer located on the barchanoid dune remained at the top of the dune, on the rather flat summit of the stoss slope, where wind speeds are known to exhibit minimal variation (Baddock et al., 2011).

The topographic profiles of the two dunes on which wind measurements are taken are acquired through photogrammetric analysis of aerial pictures captured from an unmanned aerial vehicle (UAV, drone). The grain size distribution and the associated mean grain size are obtained from granulometric sampling on these two dunes. Conducting topographical surveys on the scale of the dune field was logistically unfeasible at the time. Then, the morphodynamics of the dune population in the neighborhood are analyzed from satellite images using two images taken at a time interval of 15 years, on October 24, 2005, and December 11, 2020. For this time period, Δt, the migration and elongation distance, m and e, are estimated from the position of the migrating and elongating dunes. A triangular dune shape and transverse dune slopes of 15° are assumed to derive the height of individual elongating dunes from their width measured on satellite imagery. Similarly, an avalanche slope of 35° is used to derive the height of individual migrating dunes from the horizontal length on their longitudinal slip face. All dune properties derived from field measurements or remote sensing data are compared with the predictions of the model proposed by Courrech du Pont et al. (2024) using the surface wind data from the ECMWF ERA5-Land reanalysis (Muñoz-Sabater et al., 2021). These reanalysis data are computed for a flat sloped surface with an associated sub-grid roughness length scale, providing hourly predictions of the 10-meter wind velocity and direction at a spatial resolution of $0.1^{\mathrm{o}} \times 0.1^{\mathrm{o}}$. Based on the extent of the dune field, all results from the present study are consistent for two distinct locations, (92.9°E, 36.9°N) and (92.9°E, 37°N). In the dune model, fully described in the Supporting Information (Supporting Text 1), both dune orientations and dynamics are computed from the wind and the sand flux at the crest using the speed-up effect described in Eq. (3).

3. Estimation of the fractional speed-up ratio

Fig. 2 shows the normal-to-crest elevation profiles of the migrating and elongating dunes, together with the wind roses recorded at their crest for two ranges of wind speed. These local wind measurements are compared to the surface wind data of the ERA5-Land reanalysis over the same time period. As the elongating dune develops from a topographic obstacle upstream (Fig. 1a), it exhibits no migration, thereby maintaining a steady-state position with a crestline that aligns with the direction of elongation (Courrech du Pont et al., 2014; Lucas et al., 2015; Rozier et al., 2019). Consequently, the anemometer remains located in the upper part of the dune despite the systematic crest reversals resulting from the alternation between flow directions under bimodal wind regimes. These conditions are not met on the stoss slope of the migrating dune, where the distance between the anemometer and the crest increases progressively according to the dune migration rate. However, over the entire duration of the wind measurements, from June 2017 to December 2019, the anemometer remains on the flatter slope upwind of the crest, limiting the change in wind speed associated with the change in the apparent dune slope upstream (Fig. 2b, Supporting Information Figure S2).

Subject to frequent wind reversals, the elongated dune has a symmetric shape with steep slopes of around 20% on either side of the crest (Fig. 2a). The migrating dune has the classical asymmetrical shape of barchans with a southeast-facing avalanche slope and a gentle stoss

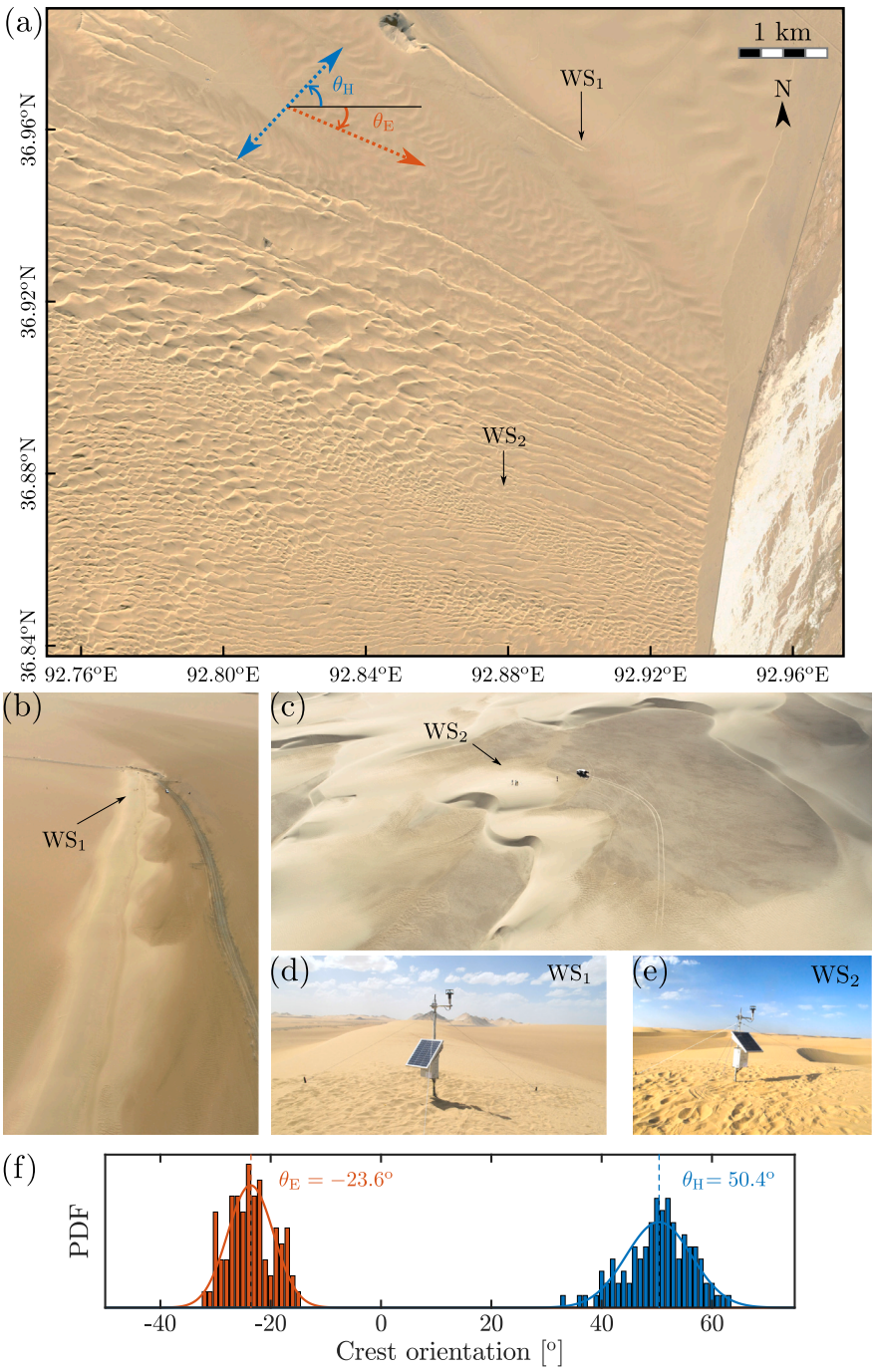

Fig. 1. Coexistence of dunes with different orientations. **(a)** Dune field on the eastern edge of the alluvial fan of the Nalinggele River (northern Qinghai-Tibet Plateau, China). Steep terraces and high river flows erase aeolian bedforms and prevent dunes from migrating or elongating east-southeast. The inset shows the orientations, θ_H and θ_E, of migrating and elongating dunes, respectively. **(b)** An elongating linear dune with a longitudinal alignment. **(c)** A migrating barchanoid ridge with a transverse alignment. Car tracks give scale and show the armoring of the interdune areas (Gao et al., 2016). **(d, e)** Zoom in on the wind towers located at the crest of these dunes, ≈ 4 km apart. **(f)** Orientation distribution of migrating (blue) and elongating (red) dunes.

slope of around 12% almost perpendicular to the primary wind (Fig. 2b). The wind roses for wind speeds above 5 $\mathrm{m\,s^{-1}}$ show that the distributions of wind orientation are similar for both dunes and the ERA5-Land data, allowing for the distinction of the two prevailing winds (Fig. 2c). For lower wind speeds, the wind roses observed at the dune crest are significantly different from each other, and also differ from the predictions of the ERA5-Land reanalysis. While the reanalysis data, computed for a flat surface, continue to show the two prevailing winds, the local measurements exhibit distinct unimodal distributions with modes that align with the corresponding crest orientation. This clearly indicates that, as a consequence of the speed-up effect, the proportion of low wind speeds perpendicular to the crest is reduced for both migrating and elongating dunes. These changes in the shape of the wind roses can be reproduced numerically from the surface winds of the ERA5-Land reanalysis (Supporting Information Figure S3), taking into account the speed-up effect and the orientation of the dunes (Eq. (3)).

Such a concrete manifestation of the impact of topography on wind speed can now be studied quantitatively using the speed-up formula (Eq. (3)). For two wind speed measurements, u_{WS_1} and u_{WS_2}, taken at

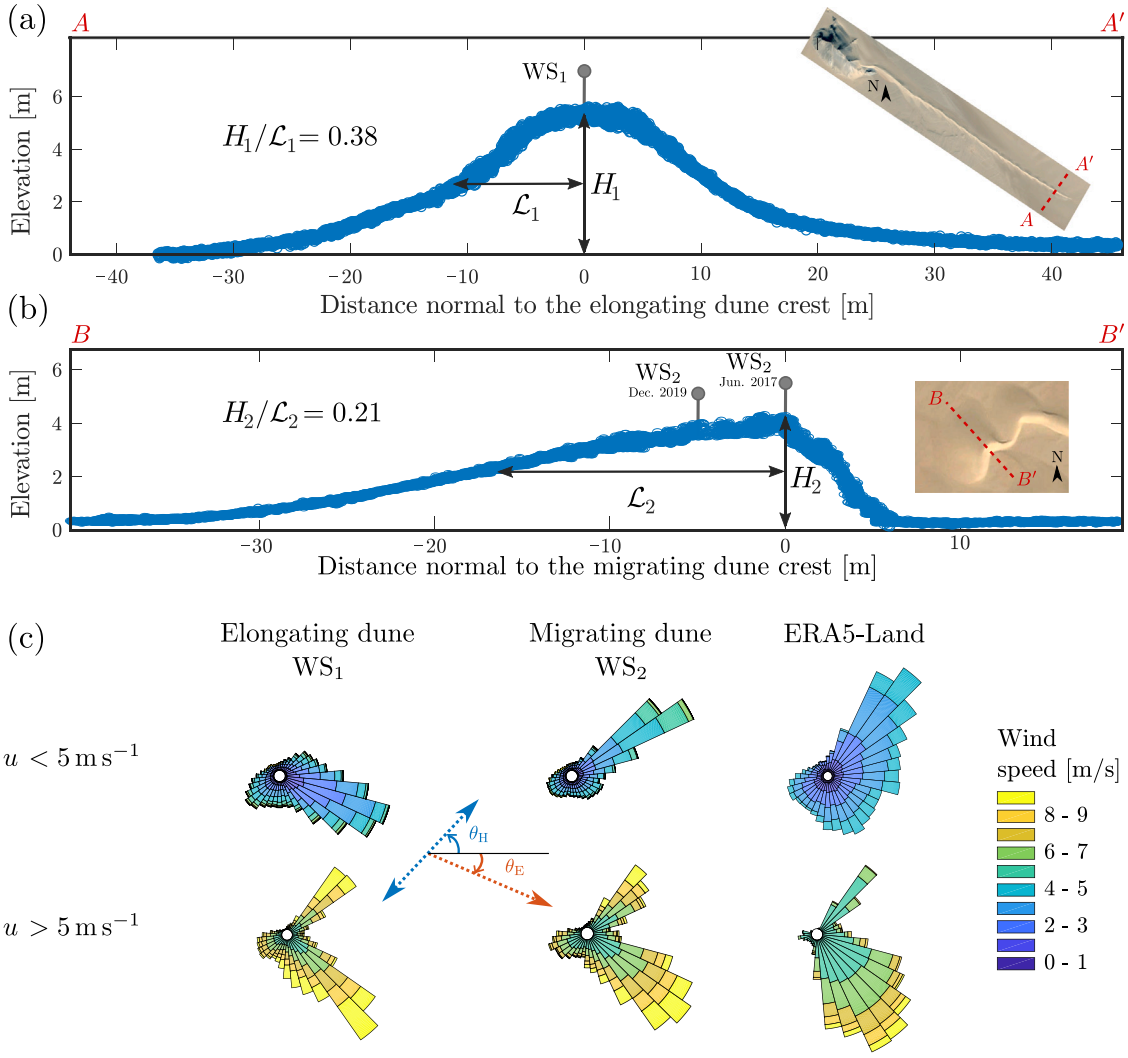

Fig. 2. Wind at the crest of dunes with different shapes and orientations. Normal-to-crest elevation profile of the **(a)** elongating and **(b)** migrating dunes. H is the dune height, $\mathcal{L}$ the half-height dune length. The elevation profiles are generated from UAV photogrammetry with a vertical resolution of 0.1 m **(c)** Wind roses at the crest of the elongating (left) and migrating (middle) dunes are compared with each other and with near-surface winds of the ERA5-Land reanalysis (right) for wind speed less (top) and greater (bottom) than 5 m s^{-1}. Wind roses indicate the direction toward which the wind blows. The inset shows the mean crest orientations observed in the field (Fig. 1). For both dune alignments, the deficit of low wind speeds in the normal-to-crest directions is a concrete manifestation of the speed-up effect.

the same height on the crest of dunes with orientations θ_E and θ_H, this formula predicts wind speed ratio of

$$\frac{u_{WS_1}}{u_{WS_2}} = \frac{1+\beta_1 H_1/\mathcal{L}_1|\sin(\theta-\theta_E)|}{1+\beta_2 H_2/\mathcal{L}_2|\sin(\theta-\theta_H)|}, \quad (4)$$

where β_1 and β_2 are assumed to be two independent dimensionless coefficients due to the difference in shape between the elongating and the migrating dunes. Due to the absence of reference wind measurements obtained from a flat bed located far from any topography, the available data cannot be used to estimate the wind deflection and speed-up at the crest of individual dune (Supporting Information, Figure S4). However, the wind speed ratio, u_{WS_1}/u_{WS_2}, can be computed at all time steps of the wind data to examine its dependence on wind direction. Then, if the dune morphology is known, $\{\beta_1, \beta_2\}$ are the only free parameters of the model described in Eq. (4).

Using the 30 months of synchronized wind data, we select only the times when the wind speed is greater than $u_{min} = 8$ m s^{-1} for at least one wind station (1.05×10^5 individual measurements, 8% of the total). Fig. 3a, b shows the ratio u_{WS_1}/u_{WS_2} according to the wind direction at the crest of the elongating dune. Although the data is scattered due to the turbulent nature of the flow, an oscillating signal emerges over the entire range of wind orientation. More than 95% of the data are between 0.2 and 2.5 and net changes in behavior are associated with the observed dune orientations. Using a sliding window algorithm with a narrow range of wind orientations (0.1°), all the quantiles of the distributions of u_{WS_1}/u_{WS_2}-values confirm the oscillating nature of the signal and the presence of various inflection points (gray curves in Fig. 3b). These observations can be directly compared to the model proposed in Eq. (4) (Fig. 3c). There is a reasonable agreement between the model and the data for $\beta_1 = 1.46$ and $\beta_2 = 1.93$. However, as might have been anticipated, the wind data do not corroborate the existence of abrupt discontinuities that would result from the two straight crest orientations of the model. Hence, a Gaussian smoothing with a standard deviation, $s_G = 30°$, is applied to the model predictions to account for the natural dispersion in the morphology of dune ridges, including crest reversals and varying slopes, as well as flow deflection (Fig. 1f). This smooth version of the model is in better agreement with the data over the entire range of wind direction (Fig. 3c), particularly capturing the sinusoidal variations observed for all quantiles of the u_{WS_1}/u_{WS_2} distributions. Throughout the observation period, no change in behavior can be distinguished, despite the relative migration with respect to the crest of the anemometer on the stoss slope of the barchanoid dune, and

Table 1
Shear velocity, sand fluxes and dune orientations derived from wind data. Surface wind data are provided by the ERA5-Land climate reanalysis at (92.9°E, 36.9°N) from January 1, 2010 to December 31, 2019. See Supporting Text 1 for the description of all variables and the values of the various environmental parameters used in the calculation, including air and grain density, and aerodynamic roughness. Angles are measured counterclockwise from East. Dune properties are computed for a range of δ-values corresponding to the fractional speed-up ratios derived from wind measurements in the field (Fig. 3c).

Shear velocity			
Mean shear velocity $\langle u_* \rangle$	m s^{-1}	0.23	
Threshold shear velocity u_c	m s^{-1}	0.18	
$\langle u_* \rangle / u_c$	ø	1.30	
Flux on a flat sand bed			
DP = $\langle \|\|\vec{Q}_{flat}\|\| \rangle$	m^2 yr^{-1}	11.1	
RDP = $\|\|\langle \vec{Q}_{flat} \rangle\|\|$	m^2 yr^{-1}	8.1	
RDP/DP	ø	0.73	
RDD	mod 360°	316.6	
Dune orientations and flux at the crest		$\delta = 0.3$	$\delta = 0.6$
Dune orientation α_H	mod 180°	42.3	45.2
Dune orientation α_E	mod 360°	325.1	329.9
$\|\|\langle \vec{Q}_H \rangle\|\| = \|\|\langle \vec{Q}_{crest}(\alpha_H) \rangle\|\|$	m^2 yr^{-1}	19.1	34.1
Direction of $\langle \vec{Q}_H \rangle$, α_M	mod 360°	313.7	313.5
$\|\|\langle \vec{Q}_M \rangle\|\| = \|\|\langle \vec{Q}_H \rangle\|\| \times \|\sin(\alpha_M - \alpha_H)\|$	m^2 yr^{-1}	19.1	34.1
$\|\|\langle \vec{Q}_E \rangle\|\| = \|\|\langle \vec{Q}_{crest}(\alpha_E) \rangle\|\|$	m^2 yr^{-1}	12.8	19.9
$\sigma_E/\sigma_H = \sigma(\alpha_E)/\sigma(\alpha_H)$	ø	0.70	0.68

the associated change in height of the wind measurements (Supporting Information, Figure S5).

A fair agreement between the model and the data is observed for all ranges of wind speed as soon as $u_{min} > 5$ m s^{-1} (Supporting Information, Figure S6). Based on a least squares best fit procedure, there is a systematic positive dependency between the β-values and the standard deviation, s_G, of the Gaussian smoothing (Supporting Information, Figure S7). Regardless of the degree of smoothing, β_1-values increase with u_{min}, while those of β_2 decrease. Considering large range of u_{min} and s_G-values, the data can be reasonably explained by $0.9 < \beta_1 < 2$ and $0.9 < \beta_2 < 2.8$, with β_1 slightly smaller than β_2, but with uncertainties that prevent rejecting the hypothesis that the two are equal. According to the measured dune aspect-ratio, $H_1/\mathcal{L}_1$ and $H_2/\mathcal{L}_2$ (Fig. 2), the fractional speed-up ratio, δ, is close to 0.5 in both cases, although extreme values of 0.2 or 0.7 cannot be excluded by the data (Supporting Information, Figure S7).

4. Dune morphodynamics

When the dune model is implemented using the δ-value estimated from short-term local wind measurements, the wind speed at the crest and the associated sand fluxes leading to migration or elongation can be estimated from the long-term ERA5-Land reanalysis surface wind speed and compared to dune morphodynamics observations (Fig. 4a, b). There are no major differences in grain size distribution for migrating and elongating dunes (Fig. 4c), so we assume the same grain diameter $d = 180$ μm and the same aerodynamic roughness $z_a = 10^{-3}$ m for both dune types. These values are identical to those used in the worldwide examples analyzed by Courrech du Pont et al. (2024). Nevertheless, we have here to take into account the high elevation of the Tibetan plateau (> 2 000 m), and we use an air density of $\rho_f = 0.9$ kg m^{-3}.

As shown in Table 1, the predicted dune orientations, α_H and α_E, for the migrating and the elongating dunes are close to the observed dune alignments θ_H and θ_E (Fig. 1f, Supporting Information, Figure S8). Despite a relatively high RDP/DP-value, the growth rate ratio $\sigma_E/\sigma_H = 0.7$ between these two dune types is within the range of values over which the two modes of dune orientation can usually coexist (Gao et al., 2015). The average sand flux $\langle \vec{Q}_E \rangle$ at the crest of elongating dune is parallel to the dune alignment, so that its magnitude governs elongation (Lucas et al., 2014). Fig. 4d shows that the predictions of the model for $\|\langle \vec{Q}_E \rangle\|$ are of the same order as those estimated from individual dune elongation rates observed in satellite images ($\|\langle \vec{Q}_E \rangle\| = eH/\Delta t$, Fig. 4a). Indeed, 90% of the $\|\langle \vec{Q}_E \rangle\|$-values derived from observations lie within the range of values predicted by the model using $0.3 \leq \delta \leq 0.6$. The average sand flux at the crest of migrating dunes $\langle \vec{Q}_H \rangle$ can be oblique to alignment, but it always determines the direction of migration α_M. Once again, the predicted α_M-value lies within the range of the dune migration direction observed in the field, which varies by almost 30° around the southeast (Fig. 4e). Only the normal-to-crest sand flux $\langle \vec{Q}_M \rangle$ contributes to dune migration, and it is given by the projection of $\langle \vec{Q}_H \rangle$ perpendicular to the crest orientation α_H. Fig. 4f shows that the values of the normal-to-crest sand flux predicted by the model using $0.3 \leq \delta \leq 0.6$ are consistent with more than 50% of the observations. These observations are based on estimates of the height and migration rate of barchanoid ridges measured on satellite imagery (Fig. 4b), $\|\langle \vec{Q}_M \rangle\| = cH/\Delta t$. As might be expected given the complexity of mass exchanges between individual dunes within a population, the sand flux derived from remote sensing data varies significantly, with a range of over one order of magnitude from 5 to 50 m^2 yr^{-1}. The mean normal-to-crest sand flux of 21.2 m^2 yr^{-1} measured in the dune field corresponds to a δ value of 0.33 in the dune model.

5. Discussion

This study demonstrates that the speed-up effect and its dependence on the aspect-ratio of the obstacle can be quantified using long-term wind data acquired at the crest of dunes with different orientations. This result, obtained from dunes several kilometers apart on an alluvial fan, highlights the spatial consistency of strong wind conditions at the scale of dune fields where there is no significant topographical disturbance. However, for a more detailed analysis of both the local wind variations and the disturbances in wind strength and direction on dunes of different types, closer dunes and wind measurements on flat beds near each of the study sites would be necessary. These field investigations will help evaluate the predictions of climate reanalyses, which will continue to offer thorough descriptions of surface wind regimes at increasingly detailed levels. When combined with the two modes of dune orientation, this effort can be extended to the length scale of active bedforms, providing a more comprehensive picture of surface flow on the complex topography of dune fields.

At this stage, given the location of the wind stations and the turbulent nature of the flow, it is necessary to average the wind data over an extended period of time in order to obtain accurate results. A solution could be to analyze how the wind-speed ratio of observed and reanalysis winds depends on wind orientation. However, systematic shifts persist between wind speed and direction measured in the field and those predicted by climate reanalysis (Supporting Information, Figure S4, and Figure 3 in Gadal et al., 2022). This issue, pertaining to the time resolution of global reanalysis, precludes accurate synchronization with field data and the direct use of surface winds as an instantaneous measure of wind on a flat bed.

Furthermore, the dune model under consideration does not fully reflect the actual complexity of dune geometry, as it is based on the assumption of an infinite linear dune with a triangular shape and identical slopes on both sides of the crest. As shown in Gao et al. (2021), a better solution would be to account for the precise dune morphologies and their fluctuations over time in accordance with crest reversals, taking into account the vertical structure of the flow and the thickness of the inner layer. The implementation of these solutions is not only challenging but also results in more intricate theoretical predictions that our data are currently unable to discern, particularly with regard to the estimation of the fractional speed-up ratio. However, despite the simplifying assumptions that have been made, we obtain β-values between 0.9 and 2.8, which is the current range of values commonly

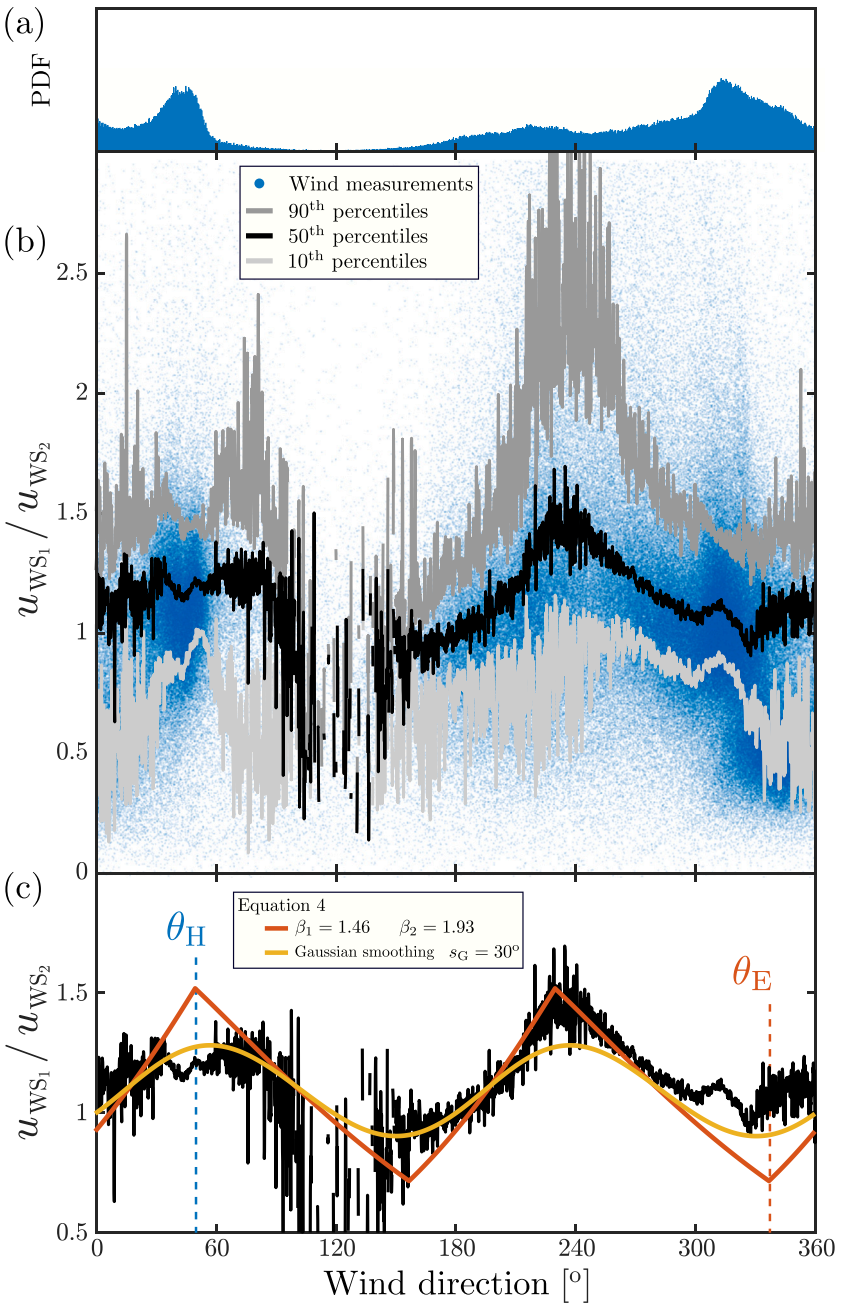

Fig. 3. Wind speed ratio at the crest of dunes as a function of wind direction. **(a)** Distribution of wind direction at the crest of the elongating dune. The wind speed direction is measured anticlockwise from east. **(b)** Ratio of synchronized wind speeds at the crest of the elongating and migrating dunes as a function of wind direction (blue dots). Only times with wind speeds greater than $u_{min} = 8\ m\ s^{-1}$ for at least one wind measurement are used. The quantiles of wind speed ratio (gray dots) are computed every 0.1° using a sliding window algorithm with an angular range of 0.2°. **(c)** Comparison between the measured and predicted wind speed ratios using a symmetric triangular dune shape (Eq. (4)) and the observed dune orientations, θ_H and θ_E (Fig. 1f). Fractional speed-up ratios $\delta_1 = \beta_1 H_1/\mathcal{L}_1 = 0.55$ and $\delta_2 = \beta_2 H_2/\mathcal{L}_2 = 0.40$ provide the best fit to the data.

reported in the field or in laboratory experiments (see Finnigan et al. (2020) and references within). Then, given the measured aspect ratio of the dunes ($H/\mathcal{L} = \{0.21, 0.38\}$, Fig. 2a) and the constraints imposed by dune dynamics, the value of the fractional speed-up ratio is found to be approximately 0.5, which is also consistent with previous observations.

Independently of the sensitivity to the fractional speed-up ratio, it is found that theoretical models of dune dynamics, together with the surface wind data computed by a climate reanalysis, can provide an accurate quantitative picture of dune evolution over a 15-year period. This includes the shape and orientation of the two main types of dunes observed in the field, as well as their migration and elongation rates and directions. All of these properties and quantities are dependent on the distribution of sand flux orientation at the crest, which may differ significantly from that on a flat bed according to the speed-up effect (Fig. 3, Supporting Information, Figure S3). This is why there is an increasing need for direct measurements of sand flux as a function of wind direction to complement the wind data like the one presented here. This work is currently being carried out by different scientific communities, mainly on coastal foredunes in the specific conditions of wet marine environments (Rotnicka, 2013; de Vries et al., 2014; Davidson-Arnott et al., 2018; Castelle et al., 2019; Schwarz et al., 2021; Bauer et al., 2022; Lamy et al., 2024). In this context, measuring the speed-up effect is made more difficult by the various factors affecting the aerodynamic roughness (e.g., plant canopy, heterogeneous

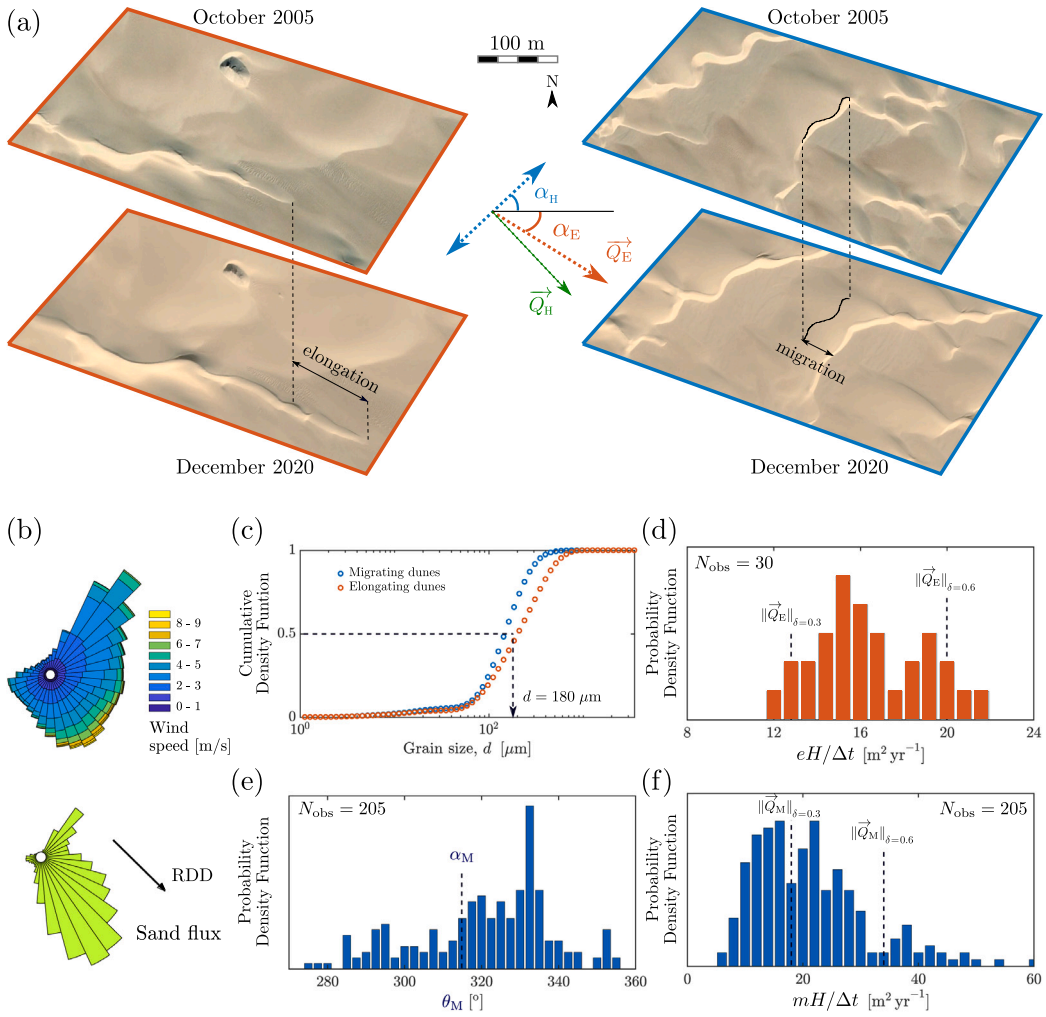

Fig. 4. Comparisons between observed and predicted dune morphodynamics. Observations are derived from satellite images, predictions are computed from the dune model using ERA5-Land surface wind data at (92.9°E, 36.9°N) from January 1, 2010 to December 31, 2019 (Supporting Text 1). All parameter values are presented in Table 1 using $\delta = \{0.3, 0.6\}$ according to β-values derived from field wind data (Fig. 3) and dune aspect ratios (Fig. 2). **(a)** Examples of dune elongation, e, and dune migration, m, over 15 years ($\Delta t = 15.13$ yrs). **(b)** Wind and sand flux roses over the same time period. They indicate the direction toward which the wind blows and the sand is transported. **(c)** Grain-size distribution over elongating and migrating dunes. **(d)** Comparison between the predicted, $\|\langle\vec{Q}_E\rangle\|$, and the observed sand flux at the crest of elongating dunes, $eH/\Delta t$. The dune height is estimated from dune width using a symmetric triangular dune shape with slopes of 15°. **(e)** Comparison between the predicted, α_M, and the observed directions of dune migration. **(f)** Comparison between the predicted, $\|\langle\vec{Q}_M\rangle\|$, and the observed sand flux at the crest of migrating dunes, $cH/\Delta t$. The dune height is estimated from the length of the avalanche slope, using an avalanche slope of 35°.

surfaces) or sand transport properties (vegetation, moisture, cohesion). In that respect, the two modes of dune orientation and synchronous measurements in hyperarid environments provide the opportunity to conduct these quantitative analysis in the absence of vegetation and humidity while using different dune alignments on the same site.

6. Conclusion

The present study focuses on the speed-up effect at the dune crest in a complex dune field submitted to a multidirectional wind regime. Long-term field measurements of wind speed demonstrate that a simplified geometric law, which assumes symmetric dunes, no crest reversal, and a constant dune aspect ratio, can reasonably predict the feedback of dune topography on flow strength. Based on the values of the fractional speed-up ratio derived from observations, new generation dune models using climate reanalysis data can estimate sand transport at the dune crest to predict with reasonable agreement a wide range of dune properties observed in the field, including orientation, migration, elongation, and growth rates. Taking advantage of the two modes of dune orientation, it is possible to provide an additional set of constraints on dune morphodynamics, which improve the comparisons between model predictions and field observations. The present study thus underscores the necessity of incorporating field data when parameterizing theoretical models to enhance their predictive capabilities and more accurately represent complex dune fields.

CRediT authorship contribution statement

Ping Lü: Writing – review & editing, Validation, Supervision, Resources, Project administration, Methodology, Investigation, Funding acquisition, Data curation. **Clément Narteau:** Writing – review & editing, Writing – original draft, Validation, Software, Methodology, Investigation, Funding acquisition, Formal analysis, Conceptualization. **Fang Ma:** Writing – review & editing, Investigation, Data curation. **Jeanne Alkalla:** Writing – review & editing, Software, Methodology, Investigation. **Zhibao Dong:** Writing – review & editing, Supervision, Funding acquisition.

Declaration of competing interest

The authors declare that they have no known competing financial interests or personal relationships that could have appeared to influence the work reported in this paper.

Acknowledgments

We acknowledge financial support from National Natural Science Foundation of China Grants 42271006 and 42241110, Laboratoire d'Excellence UnivEarthS Grant ANR-10-LABX-0023, Initiative d'Excellence Université Paris Cité Grant ANR-18-IDEX-0001, and the French National Research Agency Grants ANR-23-CE56-0008. This collaboration is a product of the French Chinese International Laboratory on Sediment Transport and Landscape Dynamics. We thank Jean Vérite for useful discussions on the topics in this paper.

Appendix A. Supplementary data

Supplementary material related to this article can be found online at https://doi.org/10.1016/j.geomorph.2025.110031.

Data availability

Data will be made available on request.

References

Arens, S., Van Kaam-Peters, H., Van Boxel, J., 1995. Air flow over foredunes and implications for sand transport. Earth Surf. Process. Landf. 20, 315–332.

Baddock, M., Livingstone, I., Wiggs, G.F., 2007. The geomorphological significance of airflow patterns in transverse dune interdunes. Geomorphology 87, 322–336.

Baddock, M.C., Wiggs, G.F., Livingstone, I., 2011. A field study of mean and turbulent flow characteristics upwind, over and downwind of barchan dunes. Earth Surf. Process. Landf. 36, 1435–1448.

Bagnold, R.A., 1941. The Physics of Blown Sand and Desert Dunes. Chapman and Hall, London.

Bauer, B.O., Davidson-Arnott, R.G., Walker, I.J., Hesp, P.A., Ollerhead, J., 2012. Wind direction and complex sediment transport response across a beach–dune system. Earth Surf. Process. Landf. 37, 1661–1677.

Bauer, B.O., Hesp, P.A., Smyth, T.A., Walker, I.J., Davidson-Arnott, R.G., Pickart, A., Grilliot, M., Rader, A., 2022. Air flow and sediment transport dynamics on a foredune with contrasting vegetation cover. Earth Surf. Process. Landf. 47, 2811–2829.

Bradley, E.F., 1983. The influence of thermal stability and angle of incidence on the acceleration of wind up a slope. J. Wind Eng. Ind. Aerodyn. 15, 231–242.

Britter, R., Hunt, J., Richards, K., 1981. Air flow over a two-dimensional hill: studies of velocity speed-up, roughness effects and turbulence. Q. J. R. Meteorol. Soc. 107, 91–110.

Castelle, B., Laporte-Fauret, Q., Marieu, V., Michalet, R., Rosebery, D., Bujan, S., Lubac, B., Bernard, J.B., Valance, A., Dupont, P., et al., 2019. Nature-based solution along high-energy eroding sandy coasts: preliminary tests on the reinstatement of natural dynamics in reprofiled coastal dunes. Water 11, 2518.

Chang, Q., Lai, Z., An, F., Wang, H., Lei, Y., Han, F., 2017. Chronology for terraces of the nalinggele river in the north Qinghai-Tibet Plateau and implications for salt lake resource formation in the Qaidam Basin. Quat. Int. 430, 12–20.

Chen, J., Zhang, D., Yang, X., Lehmkuhl, F., Jiang, W., 2022. The effects of seasonal wind regimes on the evolution of reversing barchanoid dunes. J. Geophys. Res.: Earth Surf. 127, e2021JF006489.

Claudin, P., Wiggs, G., Andreotti, B., 2013. Field evidence for the upwind velocity shift at the crest of low dunes. Bound. Layer Meteorol. 148, 195–206.

Courrech du Pont, S., Narteau, C., Gao, X., 2014. Two modes for dune orientation. Geology 42, 743–746.

Courrech du Pont, S., Rubin, D., Narteau, C., Lapôtre, M., Day, M., Claudin, P., Livingstone, I., Telfer, M., Radebaugh, J., Gadal, C., Gunn, A., Hesp, P., Carpy, S., Bristow, C., Baas, A., Ewing, R., Wiggs, G., 2024. Complementary classifications of aeolian dunes based on morphology, dynamics, and fluid mechanics. Earth-Sci. Rev. 255, 104772. http://dx.doi.org/10.1016/j.earscirev.2024.104772.

Daudon, C., Beyers, M., Jackson, D., Avouac, J.P., 2024. Prediction of barchan dunes migration using climatic models and speed-up effect of dune topography on air flow. Earth Planet. Sci. Lett. 648, 119049.

Davidson-Arnott, R., Hesp, P., Ollerhead, J., Walker, I., Bauer, B., Delgado-Fernandez, I., Smyth, T., 2018. Sediment budget controls on foredune height: Comparing simulation model results with field data. Earth Surf. Process. Landf. 43, 1798–1810.

de Vries, S., Arens, S., De Schipper, M., Ranasinghe, R., 2014. Aeolian sediment transport on a beach with a varying sediment supply. Aeolian Res. 15, 235–244.

Fernandez-Cascales, L., Lucas, A., Rodriguez, S., Gao, X., Spiga, A., Narteau, C., 2018. First quantification of relationship between dune orientation and sediment availability, Olympia Undae, Mars. Earth Planet. Sci. Lett. 489, 241–250.

Finnigan, J., Ayotte, K., Harman, I., Katul, G., Oldroyd, H., Patton, E., Poggi, D., Ross, A., Taylor, P., 2020. Boundary-layer flow over complex topography. Bound.-Layer Meteorol. 177, 247–313.

Gadal, C., Delorme, P., Narteau, C., Wiggs, G.F., Baddock, M., Nield, J.M., Claudin, P., 2022. Local wind regime induced by giant linear dunes: Comparison of era5-land reanalysis with surface measurements. Bound.-Layer Meteorol. 185, 309–332.

Gadal, C., Narteau, C., du Pont, S.C., Rozier, O., Claudin, P., 2019. Incipient bedforms in a bidirectional wind regime. J. Fluid Mech. 862, 490–516.

Gao, X., Narteau, C., Gadal, C., 2021. Migration of reversing dunes against the sand flow path as a singular expression of the speed-up effect. J. Geophys. Res.: Earth Surf. 126, e2020JF005913.

Gao, X., Narteau, C., Rozier, O., 2016. Controls on and effects of armoring and vertical sorting in aeolian dune fields: A numerical simulation study. Geophys. Res. Lett. 43, 2614–2622.

Gao, X., Narteau, C., Rozier, O., Courrech du Pont, S., 2015. Phase diagrams of dune shape and orientation depending on sand availability. Sci. Rep. 5, 14677.

Gunn, A., 2023. Formation and reorganization time scales of aeolian landscapes. Geology 51, 351–355.

Hesp, P.A., Davidson-Arnott, R., Walker, I.J., Ollerhead, J., 2005. Flow dynamics over a foredune at prince edward island, Canada. Geomorphol. 65, 71–84.

Hesp, P.A., Smyth, T.A., Nielsen, P., Walker, I.J., Bauer, B.O., Davidson-Arnott, R., 2015. Flow deflection over a foredune. Geomorphology 230, 64–74.

Jackson, P.S., Hunt, J.C.R., 1975. Turbulent wind flow over a low hill. Q. J. R. Meteorol. Soc. 101, 929–955.

Kennedy, J.F., 1963. The mechanics of dunes and antidunes in erodible-bed channels. J. Fluid Mech. 16, 521–544.

Lamy, A., Smyth, T.A., Robin, N., Hesp, P.A., 2024. Using computational fluid dynamics (cfd) to investigate airflow and sand transport on a human-made coastal foredune dominated by offshore wind: Impact of the shape variability. Coast. Eng. 191, 104534.

Lü, P., Narteau, C., Dong, Z., Claudin, P., Rodriguez, S., An, Z., Fernandez-Cascales, L., Gadal, C., Courrech du Pont, S., 2021. Direct validation of dune instability theory. Proc. Natl. Acad. Sci. 118, e2024105118.

Lü, P., Narteau, C., Dong, Z., Claudin, P., Rodriguez, S., An, Z., Gadal, C., Courrech du Pont, S., 2022. Coexistence of two dune growth mechanisms in a landscape-scale experiment. Geophys. Res. Lett. 49, e2021GL097636..

Lucas, A., Narteau, C., Rodriguez, S., Rozier, O., Callot, Y., Garcia, A., Courrech du Pont, S., 2015. Sediment flux from the morphodynamics of elongating linear dunes. Geology 43, 1027–1030.

Lucas, A., Rodriguez, S., Narteau, C., Charnay, B., Pont, S.C., Tokano, T., Garcia, A., Thiriet, M., Hayes, A.G., Lorenz, R.D., et al., 2014. Growth mechanisms and dune orientation on Titan. Geophys. Res. Lett. 41, 6093–6100.

Muñoz-Sabater, J., Dutra, E., Agustí-Panareda, A., Albergel, C., Arduini, G., Balsamo, G., Boussetta, S., Choulga, M., Harrigan, S., Hersbach, H., et al., 2021. era5-land: A state-of-the-art global reanalysis dataset for land applications. Earth Syst. Sci. Data Discuss. 1–50.

Neuman, C.M., Lancaster, N., Nickling, W., 1997. Relations between dune morphology, air flow, and sediment flux on reversing dunes, Silver Peak, Nevada. Sedimentology 44, 1103–1111.

Parsons, D.R., Walker, I.J., Wiggs, G.F., 2004. Numerical modelling of flow structures over idealized transverse aeolian dunes of varying geometry. Geomorphology 59, 149–164.

Ping, L., Narteau, C., Dong, Z., Zhang, Z., Courrech du Pont, S., 2014. Emergence of oblique dunes in a landscape-scale experiment. Nat. Geosci. 7, 99–103.

Rotnicka, J., 2013. Aeolian vertical mass flux profiles above dry and moist sandy beach surfaces. Geomorphology 187, 27–37.

Rozier, O., Narteau, C., Gadal, C., Claudin, P., Courrech du Pont, S., 2019. Elongation and stability of a linear dune. Geophys. Res. Lett. 46, 14521–14530.

Rubin, D., Hunter, R.E., 1987. Bedform alignment in directionally varying flows. Science 237, 276–278.

Schwarz, C., Van Starrenburg, C., Donker, J., Ruessink, G., 2021. Wind and sand transport across a vegetated foredune slope. J. Geophys. Res.: Earth Surf. 126, e2020JF005732.

Taylor, P.A., Mason, P.J., Bradley, E.F., 1987. Boundary-layer flow over low hills. Bound.-Layer Meteorol. 39, 107–132.

Vérité, J., Narteau, C., Rozier, O., Alkalla, J., Barrier, L., Courrech du Pont, S., 2025. Equilibrium distance from long-range dune interactions. Earth Surf. Dyn. 13, 23–39.

Walker, I.J., Hesp, P.A., Davidson-Arnott, R.G., Bauer, B.O., Namikas, S.L., Ollerhead, J., 2009. Responses of three-dimensional flow to variations in the angle of incident wind and profile form of dunes: Greenwich Dunes, Prince Edward Island, Canada. Geomorphology 105, 127–138.

Walker, I.J., Hesp, P., Smyth, T., 2022. Airflow dynamics over unvegetated and vegetated dunes. Treatise Geomorphol. 41, 5–453.

Walker, I.J., Nickling, W.G., 2003. Simulation and measurement of surface shear stress over isolated and closely spaced transverse dunes in a wind tunnel. Earth Surf. Process. Landf. 28, 1111–1124.

Wiggs, G.F., Livingstone, I., Warren, A., 1996. The role of streamline curvature in sand dune dynamics: evidence from field and wind tunnel measurements. Geomorphology 17, 29–46.

Zhang, D., Narteau, C., Rozier, O., Courrech du Pont, S., 2012. Morphology and dynamics of star dunes from numerical modelling. Nat. Geosci. 5, 463–467.